Supplementary Information (SI) for Journal of Materials Chemistry C.

Thermoelectric properties and figure of merit of Cu_2ZnSnS_4: Electronic supporting information

Tooba Sajid, Joseph M. Flitcroft, R. Freer, D. J. Lewis and Jonathan M. Skelton

1 Structure and phonon spectra

Table S1 Optimized lattice parameters of Cu_2ZnSnS_4 obtained in this study compared to experiments[1–4] and other theoretical studies.[5–8] For each comparison study the % differences from our values are provided in parentheses. [a] LDA functional. [b] HSE functional.

	$a = b$ [Å]	c [Å]	V [Å^3]
This work	5.383	10.748	311
Expt[1]	5.427 (+0.81%)	10.848 (+0.92%)	320 (+2.81%)
Expt[2]	5.44 (+1.05%)	10.712 (-0.34%)	317 (+1.89%)
Expt[3]	5.43 (+0.87%)	10.85 (+0.94%)	320 (+2.81%)
Expt[4]	5.42 (+0.68%)	10.86 (+1.03%)	319 (+2.51%)
Calc.[5]	5.639 (+4.54%)	11.234 (+4.33%)	357 (+12.9%)
Calc.[6]	5.383 (0%)	10.727 (-0.2%)	311 (0%)
Calc.[7] [a]	5.316 (-1.26%)	10.636 (-1.05%)	301 (-3.32%)
Calc.[7] [b]	5.448 (+1.19%)	10.857 (+1%)	322 (+3.41%)
Calc.[8]	5.327 (-1.05%)	10.665 (-0.78%)	303 (-2.64%)

2 Lattice thermal conductivity

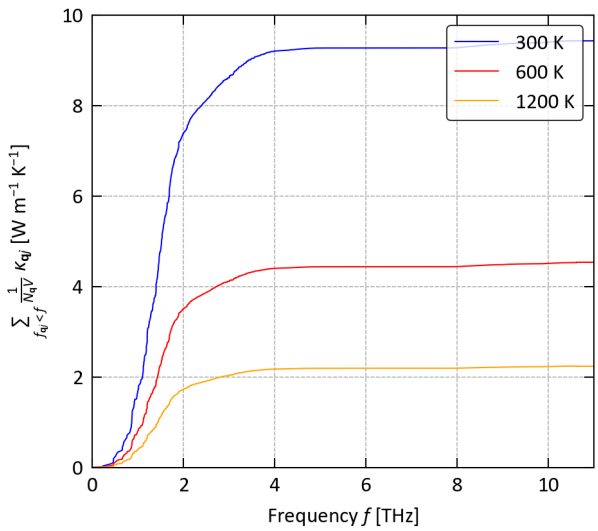

Fig. S1 Cumulative scalar-averaged lattice thermal conductivity κ_{latt} of Cu_2ZnSnS_4 as a function of phonon frequency at T = 300, 600 and 1200 K.

3 Electronic structure and transport properties

Table S2 Comparison of the calculated bandgap E_g of Cu_2ZnSnS_4 obtained in this work to previous experimental and theoretical studies. For each comparison study the % differences from our values are provided in parentheses.

	E_g [eV]
Calc. (this work)	1.279
Expt [9]	1.50 (-14.7%)
Expt [10]	1.45-1.6 (-11.8 to -20.1%)
Expt [11]	1.42-1.6 (-9.93 to -20.1%)
Calc. (HSE) [12]	1.487 (-14%)
Calc. (HSE06) [13]	1.47 (-13%)
Calc. (HSE06) [14]	1.50 (-14.7%)
Calc. (HSE06) [15]	1.44 (-11.2%)
Calc. (PBEsol) [15]	1.26 (+1.51%)
Calc. (Corrected PBE) [16]	1.281 (-0.16%)

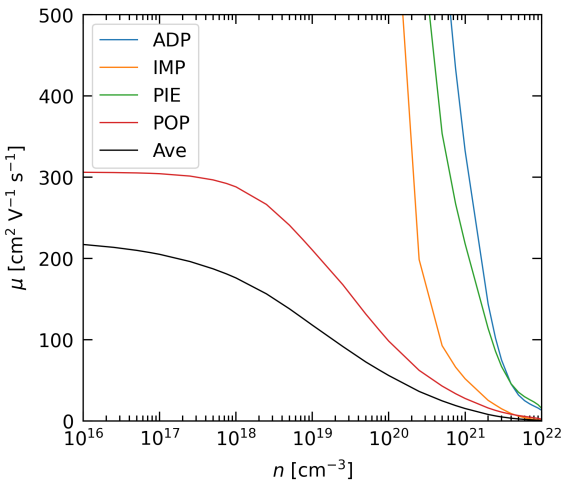

Fig. S2 Carrier mobility μ as a function of extrinsic carrier concentration ("doping level") n for p-type Cu_2ZnSnS_4 at a fixed temperature $T = 600$ K. The μ for each of the four scattering mechanisms considered in our calculations, *viz.* acoustic deformation potential (ADP), ionised impurity (IMP), piezoelectric (PIE) and polar-optic phonon (POP) scattering, are shown together with the average obtained by combining the scattering rates for all four processes. For each μ we show the scalar average defined using the equivalent of Eq. 5 in the text.

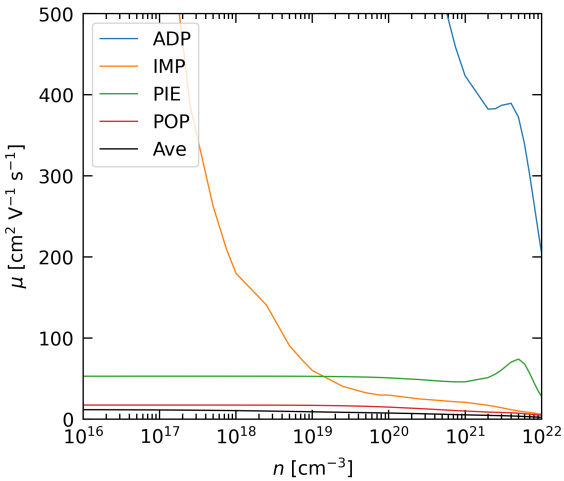

Fig. S3 Carrier mobility μ as a function of extrinsic carrier concentration ("doping level") n for n-type Cu_2ZnSnS_4 at a fixed temperature $T = 600$ K. The μ for each of the four scattering mechanisms considered in our calculations, *viz.* acoustic deformation potential (ADP), ionised impurity (IMP), piezoelectric (PIE) and polar-optic phonon (POP) scattering, are shown together with the average obtained by combining the scattering rates for all four processes. For each μ we show the scalar average defined using the equivalent of Eq. 5 in the text.

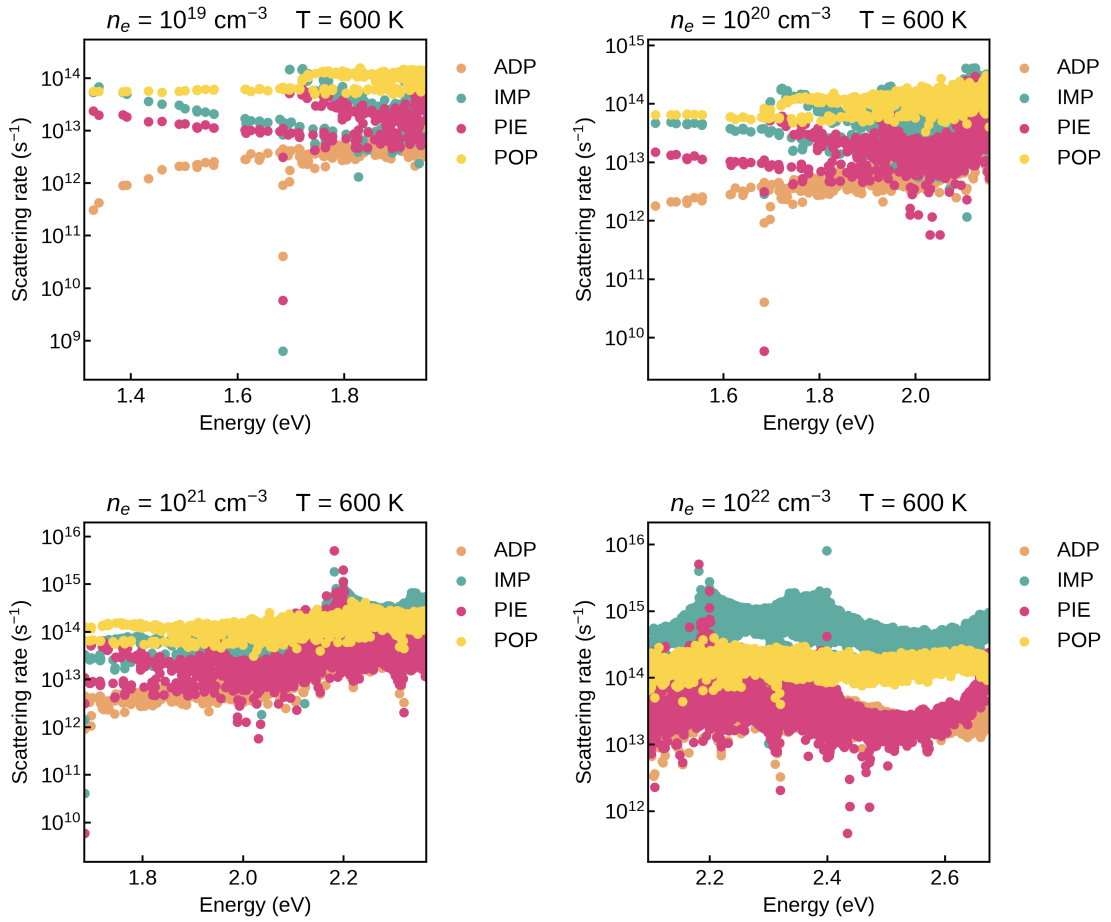

Fig. S4 Calculated electron scattering rates as a function of energy for n-type Cu_2ZnSnS_4 at $T = 600$ K and extrinsic carrier concentrations ("doping levels") $n = 10^{19}$, 10^{20}, 10^{21} and 10^{22} cm^{-3}.

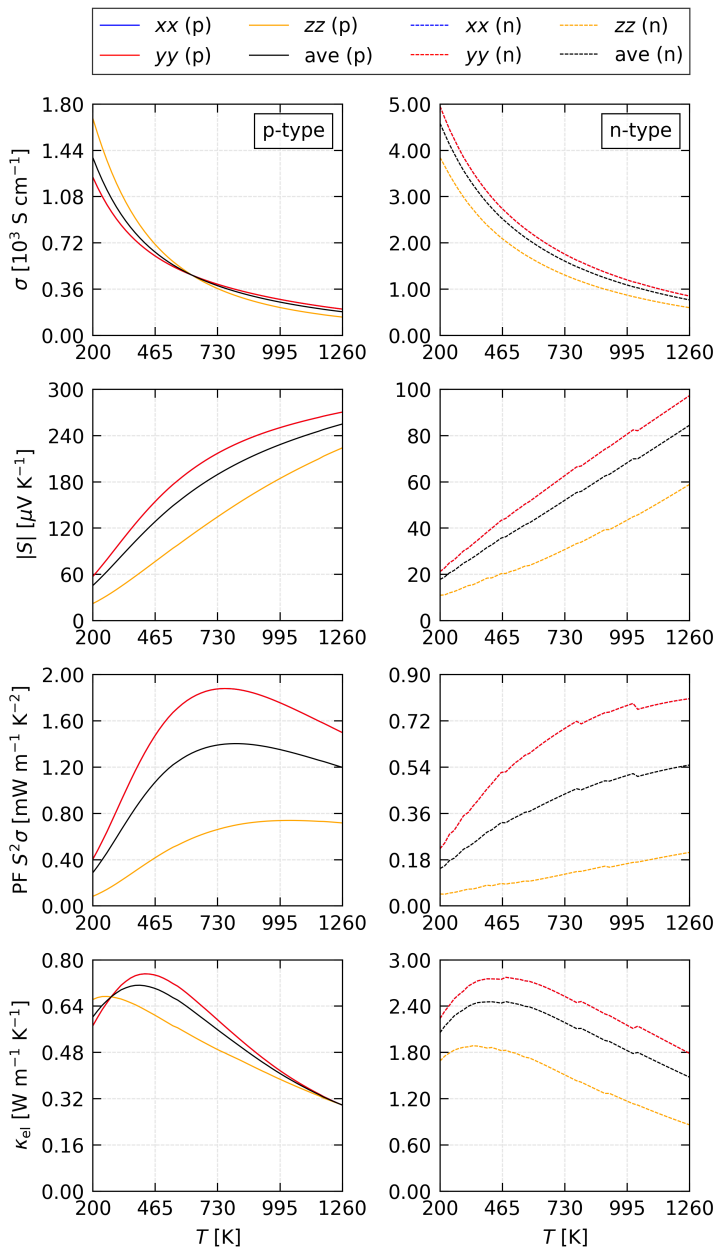

Fig. S5 Comparison of the electrical conductivity $\sigma_{\alpha\beta}$, absolute Seebeck coefficient $|S_{\alpha\beta}|$, power factor $S^2_{\alpha\beta}\sigma_{\alpha\beta}$ (PF), and electronic thermal conductivity $\kappa_{\mathrm{el},\alpha\beta}$ of bulk p-type (left) and n-type Cu_2ZnSnS_4 (right) as a function of temperature at a fixed extrinsic carrier concentration ("doping level") $n = 5\times10^{20}$ cm^{-3}. Each plot shows the diagonal xx, yy and zz elements of the tensors, corresponding to transport along the a, b and c axes, together with the scalar averages calculated using the equivalent of Eq. 5 in the text.

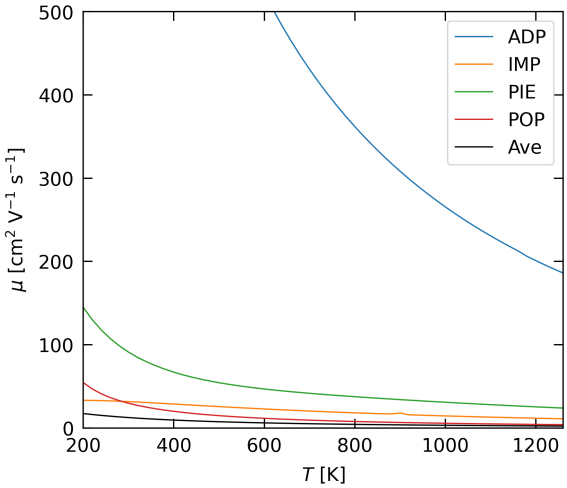

Fig. S6 Carrier mobility μ as a function of temperature T for p-type Cu_2ZnSnS_4 at a fixed extrinsic carrier concentration ("doping level") $n = 5 \times 10^{20}$ cm^{-3}. The μ for each of the four scattering mechanisms considered in our calculations, *viz.* acoustic deformation potential (ADP), ionised impurity (IMP), piezoelectric (PIE) and polar-optic phonon (POP) scattering, are shown together with the average obtained by combining the scattering rates for all four processes. For each μ we show the scalar average defined using the equivalent of Eq. 5 in the text.

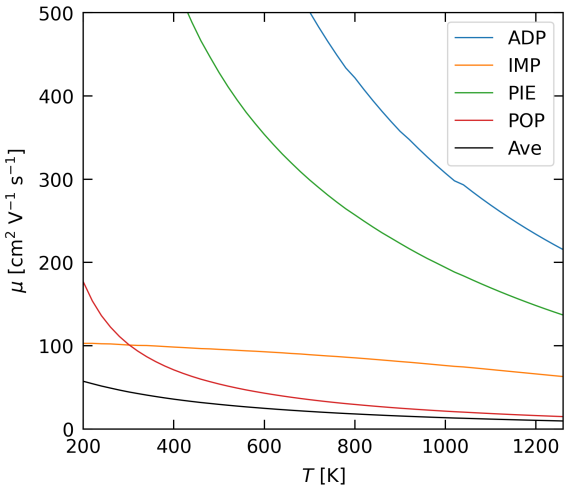

Fig. S7 Carrier mobility μ as a function of temperature T for n-type Cu_2ZnSnS_4 at a fixed extrinsic carrier concentration ("doping level") $n = 5 \times 10^{20}$ cm^{-3}. The μ for each of the four scattering mechanisms considered in our calculations, *viz.* acoustic deformation potential (ADP), ionised impurity (IMP), piezoelectric (PIE) and polar-optic phonon (POP) scattering, are shown together with the average obtained by combining the scattering rates for all four processes. For each μ we show the scalar average defined using the equivalent of Eq. 5 in the text.

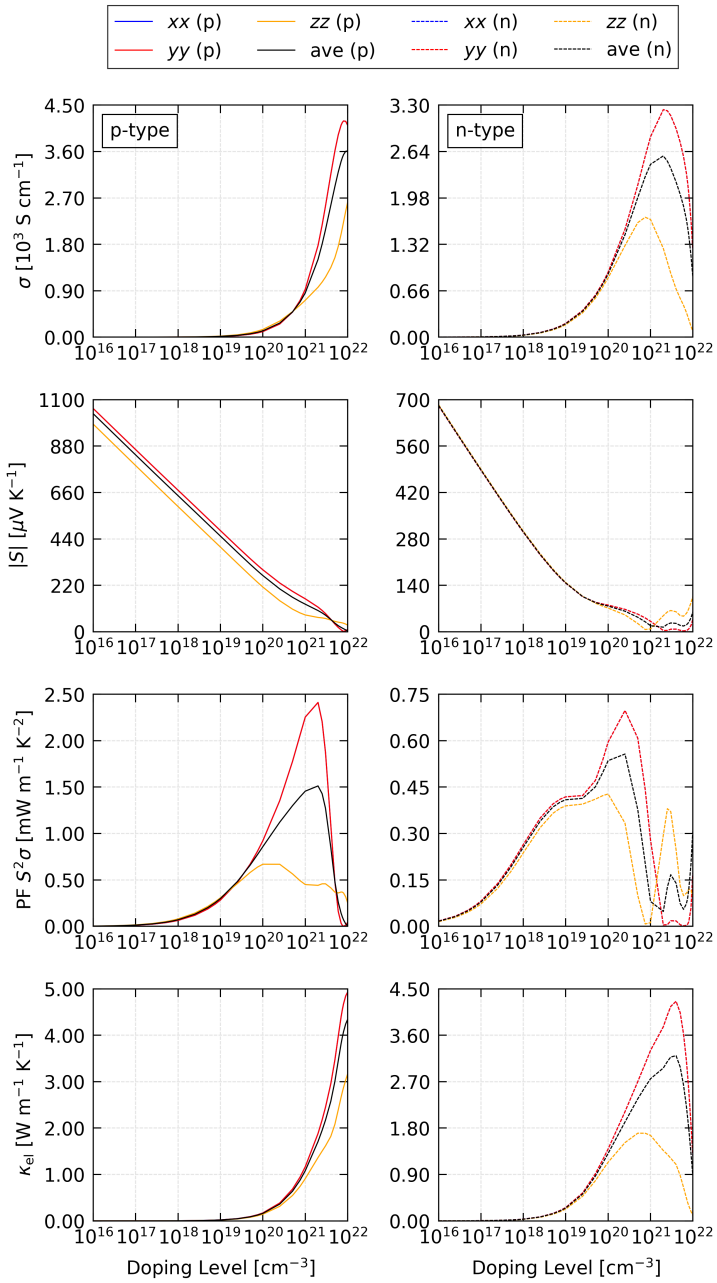

Fig. S8 Comparison of the electrical conductivity $\sigma_{\alpha\beta}$, absolute Seebeck coefficient $|S_{\alpha\beta}|$, power factor $S^2_{\alpha\beta}\sigma_{\alpha\beta}$ (PF), and electronic thermal conductivity $\kappa_{\mathrm{el},\alpha\beta}$ of bulk p-type (left) and n-type Cu_2ZnSnS_4 (right) as a function of extrinsic carrier concentration ("doping level") n at a fixed temperature T = 600 K. Each plot shows the diagonal xx, yy and zz elements of the tensors, corresponding to transport along the a, b and c axes, together with the scalar averages calculated using the equivalent of Eq. 5 in the text.

4 Thermoelectric figure of merit

Table S3 Predicted maximum scalar average figure of merit ZT_{max} of n-type Cu_2ZnSnS_4 (CZTS) at T = 400, 600 and 1000 K, corresponding roughly to the three heat-recovery scenarios outlined in Ref. 17. Predictions are given for bulk CZTS and with nanostructuring to crystallite sizes of L = 10 and 5 nm. For each prediction we show the corresponding extrinsic carrier concentration ("doping level") n, electrical conductivity σ, Seebeck coefficient S, power factor $S^2\sigma$ (PF), and electronic, lattice and total thermal conductivity κ_{el}, κ_{latt} and κ_{tot}.

			n	σ	S	$S^2\sigma$ (PF)	κ [W m^{-1} K^{-1}]		
T [K]	Crystallite size L	ZT_{max}	n [cm^{-1}]	σ [S cm^{-1}]	S [μV K^{-1}]	$S^2\sigma$ (PF) [mW m^{-1} K^{-2}]	κ_{el}	κ_{latt}	κ_{tot}
400	Bulk	0.02	2.5×10^{20}	21.1	-45.1	0.43	1.94	6.91	8.84
400	10 nm	0.05	2.5×10^{20}	12.4	-51.5	0.33	1.19	1.43	2.61
400	5 nm	0.06	2.5×10^{20}	9.1	-54.9	0.27	0.88	0.93	1.81
600	Bulk	0.06	10^{20}	8.97	-77.3	0.54	1.31	4.53	5.84
600	10 nm	0.11	2.5×10^{20}	9.64	-69.3	0.46	1.32	1.19	2.52
600	5 nm	0.13	2.5×10^{20}	7.37	-73.9	0.40	1.03	0.81	1.84
1000	Bulk	0.20	7.5×10^{19}	3.86	-135	0.70	0.83	2.69	3.52
1000	10 nm	0.35	2.5×10^{19}	1.34	-179	0.43	0.31	0.93	1.24
1000	5 nm	0.38	2.5×10^{19}	1.05	-180	0.34	0.26	0.65	0.91

1 V. Kheraj, K. K. Patel, S. J. Patel and D. V. Shah, *Journal of Crystal Growth*, 2013, **362**, 174–177.

2 T. Chandel, V. Thakur, S. Halaszova, M. Prochazka, D. Haško, D. Velic and R. Poolla, *Journal of Electronic Materials*, 2018, **47**, 5477–5487.

3 J. Guo, S. Sun, B. Liu, R. Hao and L. Sun, *Optik*, 2021, **242**, 166998.

4 M. Sahu, V. R. M. Reddy, B. Kim, B. Patro, C. Park, W. K. Kim and P. Sharma, *Materials*, 2022, **15**, 1708.

5 N. B. M. Amiri and A. Postnikov, *Physical Review B*, 2010, **82**, 205204.

6 J. A. J. and A. Walsh, *Journal of Materials Chemistry A*, 2014, **2**, 7829–7836.

7 S. P. Ramkumar, G. Petretto, W. Chen, H. P. C. Miranda, X. Gonze and G.-M. Rignanese, *Physical Review Materials*, 2022, **6**, 035403.

8 L. Boutahar, A. Benamrani, Z. Rouabah and S. Daoud, *Annals of West University of Timisoara - Physics*, 2023, **65**, 160–170.

9 S. M. Pawar, B. S. Pawar, A. V. Moholkar, D. S. Choi, J. H. Yun, J. H. Moon, S. S. Kolekar and J. H. Kim, *Electrochimica Acta*, 2010, **55**, 4057–4061.

10 H. Katagiri, K. Saitoh, T. Washio, H. Shinohara, T. Kurumadani and S. Miyajima, *Solar Energy Materials and Solar Cells*, 2001, **65**, 141–148.

11 T. Chandel, V. Thakur, S. Halaszova, M. Prochazka, D. Haško, D. Velic and R. Poolla, *Journal of Electronic Materials*, 2018, **47**, 5477–5487.

12 J. Paier, R. Asahi, A. Nagoya and G. Kresse, *Physical Review B*, 2009, **79**, 115126.

13 C. Persson, R. Chen, H. Zhao, M. Kumar and D. Huang, in *Electronic Structure and Optical Properties from First-Principles Modeling*, Wiley, 2014, pp. 75–105.

14 S. Chen, X. G. Gong, A. Walsh and S.-H. Wei, *Applied Physics Letters*, 2009, **94**, 041903.

15 C.-J. Tong, H. J. Edwards, T. D. C. Hobson, K. Durose, V. R. Dhanak, J. D. Major and K. P. McKenna, *The Journal of Physical Chemistry Letters*, 2020, **11**, 10463–10468.

16 M. Nishiwaki, K. Nagaya, M. Kato, S. Fujimoto, H. Tampo, T. Miyadera, M. Chikamatsu, H. Shibata and H. Fujiwara, *Physical Review Materials*, 2018, **2**, 85404.

17 S. LeBlanc, S. K. Yee, M. L. Scullin, C. Dames and K. E. Goodson, *Renewable and Sustainable Energy Reviews*, 2014, **32**, 313–327.